Two-Photon Rabi Splitting in a Coupled System of a Nanocavity and Exciton Complexes

Chenjiang Qian,[1,2] Shiyao Wu,[1,2] Feilong Song,[1,2] Kai Peng,[1,2] Xin Xie,[1,2] Jingnan Yang,[1,2] Shan Xiao,[1,2] Matthew J. Steer,[3] Iain G. Thayne,[3] Chengchun Tang,[1] Zhanchun Zuo,[1] Kuijuan Jin,[1,2] Changzhi Gu,[1,2] and Xiulai Xu[1,2,4,*]

[1]*Institute of Physics, Chinese Academy of Science, Beijing 100190, China*

[2]*School of Physical Sciences, University of Chinese Academy of Sciences, Beijing 100049, China*

[3]*School of Engineering, University of Glasgow, Glasgow G12 8LT, United Kingdom*

[4]*CAS Center for Excellence in Topological Quantum Computation, University of Chinese Academy of Sciences, Beijing 100190, China*

(Received 21 November 2017; published 22 May 2018)

Two-photon Rabi splitting in a cavity-dot system provides a basis for multiqubit coherent control in a quantum photonic network. Here we report on two-photon Rabi splitting in a strongly coupled cavity-dot system. The quantum dot was grown intentionally large in size for a large oscillation strength and small biexciton binding energy. Both exciton and biexciton transitions couple to a high-quality-factor photonic crystal cavity with large coupling strengths over 130 μeV. Furthermore, the small binding energy enables the cavity to simultaneously couple with two exciton states. Thereby, two-photon Rabi splitting between the biexciton and cavity is achieved, which can be well reproduced by theoretical calculations with quantum master equations.

DOI: 10.1103/PhysRevLett.120.213901

The two-photon process in quantum electrodynamics is important for investigating light-matter interaction. Similar to the single-photon process, two-photon Rabi oscillation occurs when the two-photon exchange rate between an emitter and an electromagnetic field exceeds their decay rates, providing a basis for multiphoton coherent control [1–5]. A single quantum dot (QD), containing exciton (X) and biexciton (XX) states, could serve as a two-photon emitter [6] with a long coherence time [7]. The coupled cavity-dot system can be used as a basic building block of a quantum photonic network [8–12]. However, two-photon Rabi splitting in a cavity-dot system has not yet been experimentally demonstrated, restricting its applications in multiphoton operation. This is due to the fact that the biexciton binding energy of QDs is too large in general, and coupling between the two-photon transition and cavity modes is not strong enough [13,14]. A promising way to achieve a strong-coupling regime in a cavity-dot system is to utilize a photonic crystal (PC) cavity, due to its high quality factor Q and small mode volume V [15–18].

In the past decade, PC-based cavity-dot systems have been continuously optimized for larger coupling strength and more nonlinearity features [19–23]. Nonetheless, up to now, studies have been mainly focused on a single transition and a single cavity mode. Recently, a few investigations were reported on coupled systems between cavities and two transitions from one single QD [24,25] or two different QDs [26,27]. Ota *et al.* [25] demonstrated two-photon emission enhancement, based on two single-photon strong couplings with a coupling strength of 51(43) μeV between the cavity and exciton (biexciton) state from a single QD.

In this Letter, we report on two-photon Rabi splitting in a strongly coupled cavity-dot system consisting of a nanocavity and two exciton states (X and XX) from a single QD. The obtained single-photon coupling strengths are about 130 μeV, over twice the previous value [25], which is due to the large oscillation strength and the large wave function overlapping with the cavity mode, resulting from the relatively large size of QDs [28,29]. Meanwhile, quantum confinement is weak in large QDs, leading to a small binding energy [30,31]. These make the cavity simultaneously couple to two single-photon transitions, resulting in two-photon Rabi splitting between the biexciton and cavity, which is well explained by theoretical simulations.

*L*3 PC cavities with various parameters were fabricated on a 170-nm-thick GaAs slab. InAs QDs with a density of 10^9 cm^{-2} were grown in the middle. The QDs were grown at a quite low growth rate to allow better control of the thickness for low density and to achieve a large dot size [Fig. 1(a)] for small binding energy and large oscillation strength. The temperature-dependent PL measurement was performed with a conventional confocal micro-PL setup. The overall cavity Q is around 10 000, which is high enough to achieve strong coupling in a cavity-dot system [17,18]. Figure 1(b) shows a typical cavity, and Fig. 1(c) shows a typical cavity mode with $Q = 12000$ fitted with a Lorentzian shape, which could be higher after deconvolution [32]. The details of fabrication and measurement are shown in the Supplemental Material [33].

The energy-level structure of a coupled cavity and biexciton system is shown in Fig. 1(d). Each energy level contains the QD state and the photon number in the cavity. The ground state $|G, 0\rangle$ is labeled by G. The single-exciton

 © 2018 American Physical Society

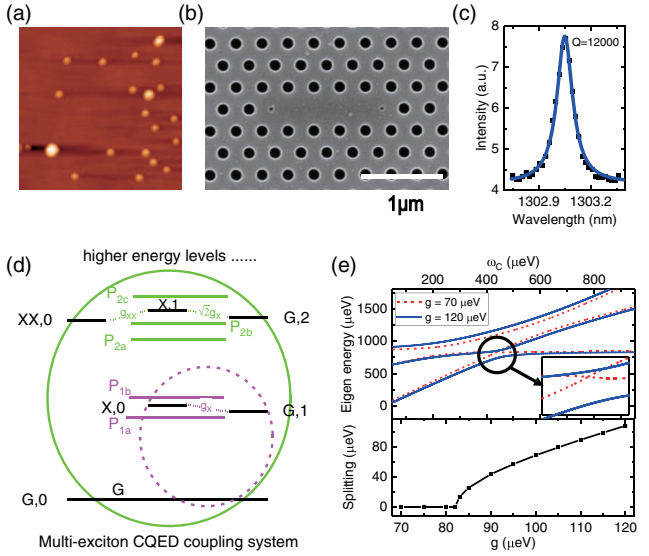

FIG. 1. (a) Atomic force microscope image of QDs in 1 μm^2. The diameter of the biggest QD is around 50 nm. (b) Scanning electron microscope image of $L3$ PC cavity. Two red circles schematize the positions of two edge holes in an unmodified $L3$ cavity. The two edge holes were optimized by a shift of $0.15\,a$ and a shrink of $0.13\,a$. (c) One-cavity mode measured at room temperature with $Q = 12000$. (d) Energy-level structure of the cavity-dot system with large coupling strength. (e) Upper panel: Calculated eigenenergies of three polaritons from coupling between $|XX,0\rangle$, $|X,1\rangle$, and $|G,2\rangle$, at $g = 70$ μeV (red dashed line) and at $g = 120$ μeV (blue solid line). Inset: Two-photon Rabi splitting occurs when $g = 120$ μeV. Bottom panel: Two-photon Rabi splitting energy as a function of g.

state $|X,0\rangle$ couples to the single-photon state $|G,1\rangle$ with g_X, forming two polaritons labeled by P_{1a} and P_{1b}. The single-exciton, one-photon state $|X,1\rangle$ couples to both the biexciton state $|XX,0\rangle$ with g_{XX} and the two-photon state $|G,2\rangle$ with $\sqrt{2}g_X$, forming three polaritons labeled by P_{2a}, P_{2b}, and P_{2c}. Similar to a three-level system in atoms [2], two-photon Rabi oscillation can be observed between $|XX,0\rangle$ and $|G,2\rangle$ when they are close to resonance, along with large coupling strengths (g_X, g_{XX}) and small biexciton binding energy. To understand this model, first we introduce a single-photon-exciton coupling system in the limit of weak excitation [34], with energy levels highlighted in the purple dashed circle in Fig. 1(d). Coupling between $|X,0\rangle$ and $|G,1\rangle$ can be described by the Hamiltonian matrix

$$\begin{pmatrix} \omega_X + \frac{i\gamma_X}{2} & g_X \\ g_X & \omega_C + \frac{i\kappa}{2} \end{pmatrix}, \tag{1}$$

where ω_X and ω_C are the eigenfrequencies of the exciton state and the cavity mode, while γ_X and κ correspond to the cavity loss and decay rate of the X transition, respectively. Two eigenvalues including the energy and decay rate of P_{1a} and P_{1b} are $(\omega_X + \omega_C)/2 + i(\gamma_X + \kappa)/4 \pm \sqrt{g^2 + (1/4)[\omega_X - \omega_C + i(\gamma_X - \kappa)/2]^2}$ [35]. Strong coupling occurs when $g > (\kappa - \gamma_X)/4$. Then we move to the biexciton system in the limit of weak excitation, as highlighted in the green solid circle. Coupling between $|XX,0\rangle$, $|X,1\rangle$, and $|G,2\rangle$ can be described by the Hamiltonian matrix

$$\begin{pmatrix} \omega_{XX} + \omega_X + i\frac{\gamma_{XX}}{2} & g_{XX} & 0 \\ g_{XX} & \omega_X + \omega_C + i\frac{\gamma_X + \kappa}{2} & \sqrt{2}g_X \\ 0 & \sqrt{2}g_X & 2\omega_C + i\kappa \end{pmatrix}. \tag{2}$$

Here, $\omega_X + \omega_{XX}$ and γ_{XX} represent the eigenfrequency and the decay rate of the biexciton state, respectively. Analytical eigenvalues of a 3×3 matrix are very complex. Instead, we choose a set of parameters $\omega_X = 600$ μeV, $\omega_{XX} = 250$ μeV, $\gamma_{XX} = \gamma_X = 5$ μeV, $\kappa = 90$ μeV to simulate numerical eigenvalues as ω_C changes from 0 to 1000 μeV with various $g_X = g_{XX} = g$. The upper panel in Fig. 1(e) shows simulated energies of P_{2a}, P_{2b}, and P_{2c} at coupling strengths $g = 70\mu$eV (red dashed line) and $g = 120$ μeV (blue solid line). Single-photon Rabi splitting occurs between the cavity and two single-photon transitions under both conditions, while two-photon Rabi splitting occurs only at $g = 120$ μeV, when $|XX,0\rangle$ and $|G,2\rangle$ are close to the resonance [as magnified in the inset in Fig. 1(e)]. The bottom panel in Fig. 1(e) shows two-photon Rabi splitting energy at different g values, indicating a threshold value of 82 μeV. Specific PL spectra simulated by solving the master equation using Quantum Optics Toolbox [36] with different coupling strengths are shown in the Supplemental Material [33].

Temperature-dependent PL spectra [Fig. 2(a)] were collected with an excitation power of 500 nW, under which both excitonic transitions and cavity mode could be observed. As temperature increases, the shift of QD emission energy could be mainly ascribed to band-gap shrinkage of the InAs QDs, following the empirical Varshni

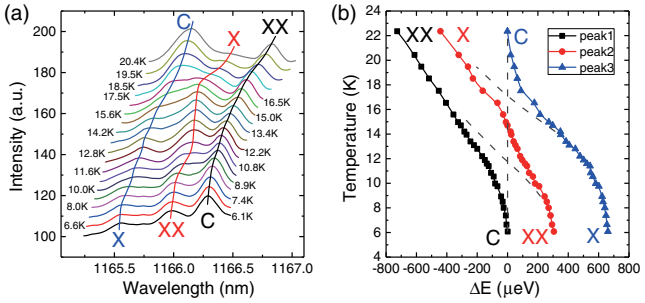

FIG. 2. (a) PL spectra of X and XX transitions and a cavity mode collected from 6 to 20 K with the excitation power of 500 nW. Peak1, peak2 and peak3 are color-coded in black, red, and blue, respectively. (b) Detuning between three peaks and bare cavity mode as a function of temperature. The detunings between uncoupled QDs and the cavity are indicated by brown dashed lines.

relation [37,38]. However, the cavity-mode energy shift is affected by two mechanisms. One is the increase of bulk refractive index, leading to a redshift [17]. The other one is the evaporating of condensed residual gas on the sample surface, resulting in a blueshift [20,39]. Figure 2(a) consists of three distinguishable peaks originating from transitions between the states formed by coherent coupling between QD excitons and the cavity mode. Peak1 is identified as the cavity mode while peak2 and peak3 are two QD transitions at 6 K. Meanwhile, peak3 is denoted as the cavity mode while peak1 and peak2 are two QD transitions at 20 K. Figure 2(b) shows the detunings (solid lines) between the three peaks and bare cavity mode as a function of temperature and compares them with uncoupled QD transitions and a bare cavity (dashed lines). PL spectrum fitting and temperature-dependent characterization of the bare cavity and QDs are shown in the Supplemental Material [33]. Clearly, two anticrossing behaviors with vacuum Rabi splitting of 246 μeV at 11 K and 242 μeV at 17 K were observed, indicating large strong coupling between the cavity and two transitions.

Strongly coupled to a cavity, the two QD peaks might originate from two QDs [26,27] or different transitions of one single QD [24,25]. To identify the two QD peaks, we first measure the excitation power-dependent PL of peak2 and peak3 at 6 K [Fig. 3(a)]. The intensity of peak2 is lower than peak3 at low excitation power, but it grows faster with increasing excitation power. The slopes of the two lines plotted logarithmically are $k_{XX} = 0.90$ and $k_X = 0.43$. $k_{XX}/k_X = 2$ manifests the characteristics of XX and X transitions of a single QD. k_{XX} (k_X) is smaller than the value of 2 (1) at extremely low excitation power [40], which might be due to the fact that the emission of QD is close to saturation in our work. The energy difference ΔE between two peaks comes from the binding energy $\chi = 350$ μeV, quite small compared with typical InAs QDs [7,13,14].

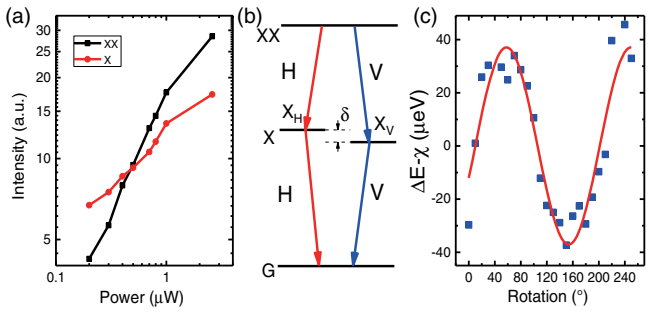

FIG. 3. (a) Peak intensity as a function of excitation power. Peak2 is weaker than peak3 at low excitation power but grows faster with increasing pumping power. (b) Four-level energy structure of QD. The X state consists of X_H and X_V with a fine-structure splitting energy δ. (c) Energy difference at different linear polarization angles. The solid red line shows a sinusoidal fitting with a π period, and the fitted fine-structure splitting energy is around 37 μeV.

Then a fine-structure splitting measurement is applied to confirm our assumption. The fine-structure splitting comes from asymmetry in the pyramidal structure of self-assembled QDs [41], as the energy-level diagram shows in Fig. 3(b). The polarization-resolved PL measurement should show an oscillation of ΔE with an amplitude of δ between the two orthogonal linear polarized emissions [42]. To perform the fine-structure splitting measurement accurately, the cavity mode is tuned away from the QD transitions to make sure that the cavity does not affect the polarization of the QD emission. Figure 3(c) shows the fitted energy difference between two peaks as a function of wave plate angle. The solid red line shows the fitted results with a sine function. The energy difference oscillates with a period of π with an amplitude of 37 μeV, which is typical for the fine-structure splitting energy of InAs QDs [43–46]. Therefore, we can conclude that peak2 and peak3 originate from the XX and X transitions of a single QD, respectively.

The contour plot of the temperature-dependent PL spectra is shown in Fig. 4(a). The single-photon Rabi splitting energies of XX-C (cavity) and X-C polaritons with values

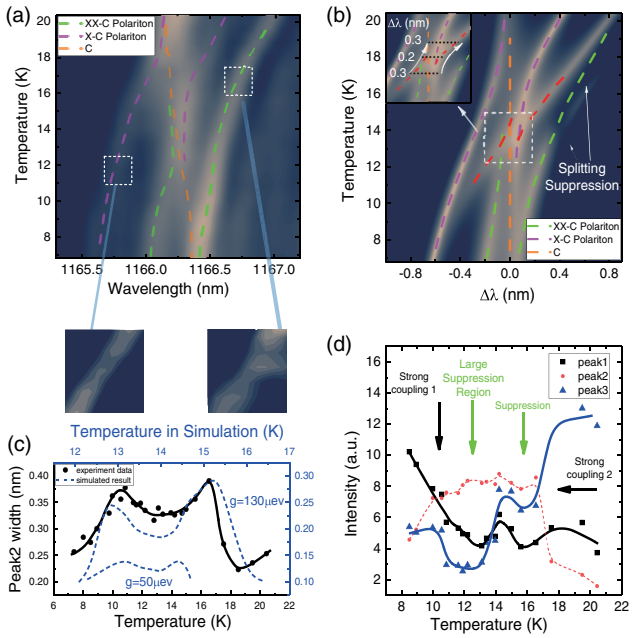

FIG. 4. (a) Contour plot of PL spectra with two suppression regions, as shown in the insets. (b) Simulated PL map with $g = 130$ μeV. The green dashed line represents the XX-C polariton, the purple dashed line shows the X-C polariton, and the orange dashed line is the bare cavity. The red dashed line is a polariton-polariton transition containing two-photon Rabi splitting. Inset: Linewidth variation during two-photon Rabi splitting. (c) Linewidth variation of peak2 at different temperatures in experiment (solid line) and calculation (dashed lines). The difference of ~0.1 nm between experimental data and calculation with $g = 130$ μeV results from the broadening of the spectrometer. (d) Intensity variation of experimental data at different temperatures. The large suppression region results from two-photon Rabi splitting.

over 240 μeV indicate large g_{XX} and g_X, leading to reversible energy exchange between the cavity and transition even with a large detuning. Due to the proximity between the single-photon Rabi splitting energies and the binding energy, the cavity could simultaneously couple to both XX and X transitions. The dynamics of this model was simulated by solving master equation using Quantum Optics Toolbox [36]. The cavity mode was set to be V-polarized, so it only coupled to V-polarized transitions (thus X_H was not considered in coupling). The cavity mode was fixed at 1166.3 nm for simplicity, and the decay rate was 90 μeV ($Q = 14000$) after deconvolution with our spectrometer's linewidth. XX and X transitions can be quadratically tuned as a function of temperature with a linewidth of 10 μeV, which was extracted from the experimental data. Due to the similarity of two single-photon Rabi splitting energies in our experimental observation, we set $g_X = g_{XX} = g$ in the calculations. Temperature-dependent PL spectra were simulated with different coupling strengths. In our system, g was obtained with a value of around 130 μeV, according to the Rabi splitting energy from the experimental results. The calculation results are shown in Fig. 4(b) on a logarithmic color scale, from which two single-photon anticrossings are observed and additional nonlinearity effects can be resolved in the region between them. Compared with our experimental data in Fig. 4(a), it can be seen that the theoretical calculation result corresponds well with experimental data. Some differences between Figs. 4(a) and 4(b) are due to the fact that the cavity mode shifts as temperature increases in experiments, while it is kept at the same position in the calculation.

The single-photon coupling strength g exceeds the threshold value of 82 μeV in our calculation in Fig. 1(e) (same binding energy and same cavity Q), indicating two-photon Rabi oscillation between $|XX, 0\rangle$ and $|G, 2\rangle$. The two-photon Rabi splitting could be clearly resolved in calculated PL mapping [Fig. 4(b)]. The green (purple) dashed line schematizes XX-C (X-C) polaritons, and the XX transition contains two splittings. The splitting at 16 K comes from the two transitions XX-P_{1a} and XX-P_{1b}, due to the single-photon splitting of $|X, 0\rangle$ and $|G, 1\rangle$ [24]. The splitting at 14 K comes from P_{2a}-P_{1b} and P_{2b}-P_{1b}, due to two-photon Rabi oscillation between $|XX, 0\rangle$ and $|G, 2\rangle$. Meanwhile, the splitting in the red lines (P_{2a}-P_{1a} and P_{2b}-P_{1a}) results from the two-photon Rabi oscillation as well. During the two-photon strong coupling, there is a large two-photon emission enhancement region, along with a large suppression region in the XX and X transitions. Specific calculations and theoretical analysis with different coupling strengths from small to large are shown in the Supplemental Material [33]. These nonlinearity features come from the built-in correlation between the XX and X transitions of one single QD, which could hardly be observed for a coupled system with one cavity and two different QDs [27].

In our experimental data, we could not distinguish every peak shown in theory, which is limited by the linewidth of our spectrometer. However, two-photon Rabi splitting could be proved from the temperature-dependent linewidth of peak2 [Fig. 4(c)]. The linewidth increases up to a maximum value of ~0.4 nm at 11 and 16 K, because at those temperatures peak2 is a combination of several peaks. In the depression region between two maximum values, the minimum linewidth is ~0.3 nm, much wider than bare cavity mode (~0.18 nm without deconvolution). The experimental linewidth variation is in good agreement with calculation results [Fig. 4(c) and the inset in Fig. 4(b)], considering the broadening of 0.1 nm from the spectrometer. In contrast, when g is small and no two-photon Rabi splitting occurs, the minimum linewidth should be almost the same as in cavity mode [see Fig. 4(c) and Supplemental Material [33]]. Additionally, two suppression regions [insets in Fig. 4(a)] are clearly observed, shown as well in the intensity variation diagram fitted from PL spectra [Fig. 4(d)]. The two PL suppression regions [green arrows in Fig. 4(d)] in single-photon emission (peak1 and peak3) are also in good agreement with our theoretical analysis above [two splittings labeled by white arrows in Fig. 4(b)]. Suppression at 16 K is due to the single-photon Rabi splitting of the XX-X_V transition, with only emission from the uncoupled XX-X_H transition left (not shown in the simulation result). The large suppression region around 13 K results from strong coupling along with emission enhancement of the two-photon process, correspondingly. In contrast, when g is small, this suppression region should reduce to a point due to weak coupling in the two-photon process [25]. On account of simulation and analysis of the experimental data, we can confirm the two-photon Rabi splitting in our coupled biexciton-cavity system.

In conclusion, we demonstrated two-photon Rabi splitting in a strongly coupled system consisting of an $L3$ PC cavity and a single embedded QD with multiple exciton states. Both XX and X transitions of the single QD were strongly coupled to one cavity mode with large coupling strengths of 130 μeV. Such a large coupling strength close to half of the binding energy 350 μeV enabled the cavity to simultaneously couple to two single-photon transitions, leading to two-photon Rabi splitting between the biexciton and cavity modes as predicted by theoretical analysis and simulation. Our work promotes the strong coupling regime in the cavity-dot system from single-photon processes to multiphoton processes, providing an approach for multiqubit operation. Additionally, our cavity-dot system can be easily integrated with PC waveguides with a wavelength approaching the telecommunication regime, which has great potential for a quantum photonic network.

This work was supported by the National Basic Research Program of China under Grant No. 2014CB921003; the National Natural Science Foundation of China under Grants No. 11721404, No. 51761145104, and No. 61675228; and

the Strategic Priority Research Program of the Chinese Academy of Sciences under Grants No. XDB07030200 and No. XDPB0803, and the CAS Interdisciplinary Innovation Team. Authors would like to thank Gas Sensing Solutions Ltd. for using the MBE equipment.

*xlxu@iphy.ac.cn

[1] T. Liang, L. Nunes, M. Tsuchiya, K. Abedin, T. Miyazaki, D. V. Thourhout, W. Bogaerts, P. Dumon, R. Baets, and H. Tsang, Opt. Commun. **265**, 171 (2006).
[2] M. Ornigotti, G. D. Valle, T. T. Fernandez, A. Coppa, V. Foglietti, P. Laporta, and S. Longhi, J. Phys. B **41**, 085402 (2008).
[3] M. Saffman, T. G. Walker, and K. Mølmer, Rev. Mod. Phys. **82**, 2313 (2010).
[4] M. Fushitani, C.-N. Liu, A. Matsuda, T. Endo, Y. Toida, M. Nagasono, T. Togashi, M. Yabashi, T. Ishikawa, Y. Hikosaka, T. Morishita, and A. Hishikawa, Nat. Photonics **10**, 102 (2016).
[5] S. Bounouar, M. Strauß, A. Carmele, P. Schnauber, A. Thoma, M. Gschrey, J.-H. Schulze, A. Strittmatter, S. Rodt, A. Knorr, and S. Reitzenstein, Phys. Rev. Lett. **118**, 233601 (2017).
[6] S. Stufler, P. Machnikowski, P. Ester, M. Bichler, V. M. Axt, T. Kuhn, and A. Zrenner, Phys. Rev. B **73**, 125304 (2006).
[7] Z. M. Wang, *Self-Assembled Quantum Dots*, Vol. 1 (Springer-Verlag, New York, 2007).
[8] H. Nakamura, Y. Sugimoto, K. Kanamoto, N. Ikeda, Y. Tanaka, Y. Nakamura, S. Ohkouchi, Y. Watanabe, K. Inoue, H. Ishikawa, and K. Asakawa, Opt. Express **12**, 6606 (2004).
[9] D. G. Angelakis, M. F. Santos, V. Yannopapas, and A. Ekert, Phys. Lett. A **362**, 377 (2007).
[10] A. Faraon, I. Fushman, D. Englund, N. Stoltz, P. Petroff, and J. Vučković, Opt. Express **16**, 12154 (2008).
[11] R. Bose, D. Sridharan, H. Kim, G. S. Solomon, and E. Waks, Phys. Rev. Lett. **108**, 227402 (2012).
[12] Y.-C. Liu, X. Luan, H.-K. Li, Q. Gong, C. W. Wong, and Y.-F. Xiao, Phys. Rev. Lett. **112**, 213602 (2014).
[13] E. del Valle, S. Zippilli, F. P. Laussy, A. Gonzalez-Tudela, G. Morigi, and C. Tejedor, Phys. Rev. B **81**, 035302 (2010).
[14] D. Heinze, A. Zrenner, and S. Schumacher, Phys. Rev. B **95**, 245306 (2017).
[15] Y. Akahane, T. Asano, B.-S. Song, and S. Noda, Nature (London) **425**, 944 (2003).
[16] K. J. Vahala, Nature (London) **424**, 839 (2003).
[17] T. Yoshie, A. Scherer, J. Hendrickson, G. Khitrova, H. M. Gibbs, G. Rupper, C. Ell, O. B. Shchekin, and D. G. Deppe, Nature (London) **432**, 200 (2004).
[18] K. Hennessy, A. Badolato, M. Winger, D. Gerace, M. Atature, S. Gulde, S. Falt, E. L. Hu, and A. Imamoglu, Nature (London) **445**, 896 (2007).
[19] S. Strauf, K. Hennessy, M. T. Rakher, Y.-S. Choi, A. Badolato, L. C. Andreani, E. L. Hu, P. M. Petroff, and D. Bouwmeester, Phys. Rev. Lett. **96**, 127404 (2006).
[20] F. S. F. Brossard, X. L. Xu, D. A. Williams, M. Hadjipanayi, M. Hugues, M. Hopkinson, X. Wang, and R. A. Taylor, Appl. Phys. Lett. **97**, 111101 (2010).
[21] D. Englund, A. Majumdar, M. Bajcsy, A. Faraon, P. Petroff, and J. Vučković, Phys. Rev. Lett. **108**, 093604 (2012).
[22] H. Kim, R. Bose, T. C. Shen, G. S. Solomon, and E. Waks, Nat. Photonics **7**, 373 (2013).
[23] S. Sun, H. Kim, G. S. Solomon, and E. Waks, Nat. Nanotechnol. **11**, 539 (2016).
[24] M. Winger, A. Badolato, K. J. Hennessy, E. L. Hu, and A. Imamoglu, Phys. Rev. Lett. **101**, 226808 (2008).
[25] Y. Ota, S. Iwamoto, N. Kumagai, and Y. Arakawa, Phys. Rev. Lett. **107**, 233602 (2011).
[26] A. Laucht, J. M. Villas-Bôas, S. Stobbe, N. Hauke, F. Hofbauer, G. Böhm, P. Lodahl, M.-C. Amann, M. Kaniber, and J. J. Finley, Phys. Rev. B **82**, 075305 (2010).
[27] H. Kim, D. Sridharan, T. C. Shen, G. S. Solomon, and E. Waks, Opt. Express **19**, 2589 (2011).
[28] R. Al-Khuzheyri, A. C. Dada, J. Huwer, T. S. Santana, J. Skiba-Szymanska, M. Felle, M. B. Ward, R. M. Stevenson, I. Farrer, M. G. Tanner, R. H. Hadfield, D. A. Ritchie, A. J. Shields, and B. D. Gerardot, Appl. Phys. Lett. **109**, 163104 (2016).
[29] L. Sapienza, R. Al-Khuzheyri, A. Dada, A. Griffiths, E. Clarke, and B. D. Gerardot, Phys. Rev. B **93**, 155301 (2016).
[30] T. Takagahara and K. Takeda, Phys. Rev. B **46**, 15578 (1992).
[31] Y. Z. Hu, S. W. Koch, M. Lindberg, N. Peyghambarian, E. L. Pollock, and F. F. Abraham, Phys. Rev. Lett. **64**, 1805 (1990).
[32] J. Jimenez-Mier, J. Quant. Spectrosc. Radiat. Transfer **51**, 741 (1994).
[33] See Supplemental Material at http://link.aps.org/supplemental/10.1103/PhysRevLett.120.213901 for the detail of the fabrication process, measurement setup, the temperature-dependent PL spectra of a weak coupled system and calculations for the model.
[34] H. J. Carmichael, R. J. Brecha, M. G. Raizen, H. J. Kimble, and P. R. Rice, Phys. Rev. A **40**, 5516 (1989).
[35] L. C. Andreani, G. Panzarini, and J.-M. Gérard, Phys. Rev. B **60**, 13276 (1999).
[36] S. M. Tan, J. Opt. B **1**, 424 (1999).
[37] Y. Varshni, Physica (Utrecht) **34**, 149 (1967).
[38] H. Lee, W. Yang, and P. C. Sercel, Phys. Rev. B **55**, 9757 (1997).
[39] S. Mosor, J. Hendrickson, B. C. Richards, J. Sweet, G. Khitrova, H. M. Gibbs, T. Yoshie, A. Scherer, O. B. Shchekin, and D. G. Deppe, Appl. Phys. Lett. **87**, 141105 (2005).
[40] K. Brunner, G. Abstreiter, G. Böhm, G. Tränkle, and G. Weimann, Phys. Rev. Lett. **73**, 1138 (1994).
[41] D. Gammon, E. S. Snow, B. V. Shanabrook, D. S. Katzer, and D. Park, Phys. Rev. Lett. **76**, 3005 (1996).
[42] R. J. Young, R. M. Stevenson, A. J. Hudson, C. A. Nicoll, D. A. Ritchie, and A. J. Shields, Phys. Rev. Lett. **102**, 030406 (2009).
[43] R. Seguin, A. Schliwa, S. Rodt, K. Pötschke, U. W. Pohl, and D. Bimberg, Phys. Rev. Lett. **95**, 257402 (2005).
[44] W. Langbein, P. Borri, U. Woggon, V. Stavarache, D. Reuter, and A. D. Wieck, Phys. Rev. B **69**, 161301 (2004).
[45] J. D. Mar, X. L. Xu, J. S. Sandhu, A. C. Irvine, M. Hopkinson, and D. A. Williams, Appl. Phys. Lett. **97**, 221108 (2010).
[46] J. D. Mar, J. J. Baumberg, X. L. Xu, A. C. Irvine, and D. A. Williams, Phys. Rev. B **93**, 045316 (2016).